Precambrian Research 427 (2025) 107851

Contents lists available at ScienceDirect

Precambrian Research

journal homepage: www.elsevier.com/locate/precamres

In situ Rb–Sr dating and REE analysis of glauconites and detrital feldspars from the Ediacaran/Cambrian strata: Centralian and Adelaide Superbasins, Australia

Cecilia Loyola [a,*], Juraj Farkaš [a,b,*], Alan S. Collins [a,b], Sarah E. Gilbert [c], Charles Verdel [d], Stefan C. Löhr [a,e], Glenn A. Brock [e], Graham A. Shields [f], Andre Baldermann [g], Ahmad Redaa [h], Morgan Blades [a], Darwinaji Subarkah [a,b], Caleb Bishop [i], Sarah M. Giles [j], Nicholas Christie-Blick [j], Peter W. Haines [k]

[a] Metal Isotope Group and Tectonics and Earth Systems, School of Physics, Chemistry and Earth Sciences, University of Adelaide, SA 5005, Australia
[b] MinEx CRC, Australian Resources Research Centre, Perth, WA 6151, Australia
[c] Adelaide Microscopy, University of Adelaide, Adelaide, SA 5005, Australia
[d] Northern Territory Geological Survey (NTGS), Alice Springs, Australia
[e] School of Natural Sciences, Macquarie University, Sydney, NSW 2109, Australia
[f] Department of Earth Sciences, University College London, WC1E 6BT, UK
[g] Institute of Applied Geoscience, Graz University of Technology and NAWI Graz Geocentre, Graz, Austria
[h] Arabian Shield Research Group, Faculty of Earth Sciences, King Abdulaziz University, Jeddah, Saudi Arabia
[i] Research School of Earth Sciences, The Australian National University, Canberra, ACT 2601, Australia
[j] Department of Earth and Environmental Sciences, and Lamont-Doherty Earth Observatory of Columbia University, Palisades, NY 10964-8000, USA
[k] Geological Survey of Western Australia, Perth, WA 6004, Australia

ARTICLE INFO

Keywords:
Proterozoic Basins
Ediacaran-Cambrian
Australia
Rb–Sr dating
REE
Glauconite
Feldspar

ABSTRACT

Proterozoic sedimentary rocks are challenging to date due to the absence of fossils for biostratigraphic constraints. This study employs in situ Rb–Sr dating of K-rich minerals (glauconite and K-feldspar) to constrain depositional and diagenetic histories within the late Proterozoic–early Paleozoic Centralian and Adelaide Superbasins, Australia. Samples analyzed include the Arumbera Sandstone (Amadeus Basin), Dey Dey Mudstone (Officer Basin), and Wonoka Formation (Flinders Ranges), spanning the Precambrian-Cambrian transition (~580–520 Ma).

In situ Rb–Sr dating of glauconite from the above depositional systems yielded ages between 422 ± 11 Ma and 472 ± 5 Ma, thus systematically younger than the expected depositional ages, reflecting diagenetic overprinting during later post-depositional tectonic events, such as the Alice Springs Orogeny (Rodingan Event, ~440–430 Ma) (Scrimgeour, 2013), and the Delamerian Orogeny (~514–480 Ma). Interestingly, a pore-filling K-rich clay material from the Arumbera Sandstone (Amadeus Basin) returned an age of 530 ± 67 Ma, aligning with the expected depositional age.

Finally, detrital K-feldspar grains from the Arumbera Sandstone provided older Rb–Sr ages (1149–1780 Ma), which are thus consistent with ages or possible source rocks from the Musgrave Province and Kimban Orogen, supported by petrographic analysis as well as distinct REE patterns. These findings demonstrate the utility of combined in situ Rb–Sr dating, petrographic and REE analyses, for investigating diagenetic processes, post-depositional tectonic events, and sediment provenance in the Proterozoic basins. This novel approach offers a direct, rapid, efficient geochronological tool for characterizing complex depositional, diagenetic and alteration/burial histories of glauconite-rich strata with minimal sample preparation.

* Corresponding authors.
E-mail addresses: cecilia.loyola@adelaide.edu.au (C. Loyola), juraj.farkas@adelaide.edu.au (J. Farkaš).

https://doi.org/10.1016/j.precamres.2025.107851
Received 4 March 2025; Received in revised form 27 May 2025; Accepted 31 May 2025
Available online 12 June 2025

1. Introduction

Proterozoic sedimentary rocks can preserve the record of marine and terrestrial near-surface processes and environmental conditions on our planet over the last ca. two billion-years, prior to the Cambrian Period and the appearance of more complex life forms and associated biomineralized macro-fossils (Eriksson et al., 1998; Holland, 2006; Knoll, 2015). To better understand these geological and biological records, and their evolution through time, it is essential to precisely date the Precambrian sedimentary archives (Cawood et al., 2012; Gehrels, 2014; Nutman et al., 2016).

Proterozoic sedimentary sequences have been successfully dated via U-Pb geochronology, which yields precise and accurate ages for volcanogenic zircons in interbedded ash deposits (e.g., Cox et al. 2018). The latter can be dated via Laser Ablation Inductively Coupled Plasma Mass Spectrometry (LA-ICP-MS) (Gray, 1985; Mokgalaka and Gardea-Torresdey, 2006; Longerich, 2008), or via a more precise solution-based and isotope dilution thermal ionisation mass spectrometry (ID-TIMS) or MC ICP MS (e.g., Cox et al., 2018; and references therein). Alternatively, siliciclastic sedimentary rocks (sandstones, etc.) containing detrital zircons can be also dated via U–Pb geochronology, where the age of the youngest zircons provides a maximum depositional age (e.g., Yang et al., 2018; Lloyd et al., 2020; Collett, 2025). In addition, organic-rich Proterozoic shales have been dated via Re–Os geochronology applied to organic matter present or deposited in the sediment (e.g., Ravizza & Turekian, 1989; Yin et al., 2023). These approaches, however, have some inherent limitations for dating sedimentary sequences, including a general lack or absence of volcanic ash beds, and the fact that detrital zircons provide maximum, rather than absolute, depositional ages, depending on the timing of volcanic activity within the investigated region(s).

Recent developments in advanced in situ dating techniques, such as U–Pb carbonate dating (e.g., Drost et al., 2018; Roberts et al., 2020; Monchal et al., 2023; Subarkah et al. 2024) and Rb–Sr or K–Ar dating of authigenic clay minerals like illite (e.g., Subarkah et al. 2022) and glauconite (e.g., Löhr et al., 2024), offer alternative ways to constrain the depositional ages of marine carbonaceous and siliciclastic sedimentary rocks. Specifically, novel in situ dating techniques developed for negative-beta decay geochronometers (Rb–Sr, K–Ca, etc), using a reaction-cell and plasma mass spectrometry (LA-ICP-MS/MS), allows a direct, rapid, efficient laser-based analysis or dating at micro-scale level, and with a minimum sample preparation (Zack & Hogmalm, 2016; Hogmalm et al., 2017; Gorojovsky and Alard, 2020; Redaa et al., 2021, 2022; Bevan et al., 2024; Neofitu et al., 2024).

Here, we apply in situ Rb–Sr dating of authigenic marine clays (glauconite) and detrital grains (K-feldspar) from the Ediacaran/Cambrian marine sedimentary sequences deposited in the Centralian (Amadeus, Officer Basins) and Adelaide (Flinders Ranges) Superbasins in Australia. This study aims to constrain the depositional ages and/or post-depositional diagenetic histories of these glauconite-bearing sedimentary rocks, and to test whether these K-rich mineral phases preserve their original Rb–Sr age, or if they have been impacted and reset by later (diagenetic, burial, tectonic/orogenic) events. In addition to Rb–Sr dating, the concentrations of Rare Earth Elements (REE) were also measured simultaneously in the above K-rich mineral phases.

2. Materials and methods

2.1. Geological setting and sampled materials and strata

This study investigates the mid-Ediacaran to early Cambrian and glauconite-bearing and sedimentary sequences, including the Dey Dey Mudstone (Officer Basin, South Australia), the Wonoka Formation (Adelaide Superbasin, South Australia), and the Arumbera Sandstone (Amadeus Basin, Northern Territory), (see Fig. 1). Glauconite is a K- and Fe-rich dioctahedral interlayer-deficient mica group mineral (Rieder et al., 1998), which precipitates from seawater or seawater-derived pore fluids in marine sediments, forming sub-mm to mm sized green pellets typically within 10 s to 100 s of thousands of years in the continental shelf settings (Giresse, 2022), commonly under sub-oxic, partially

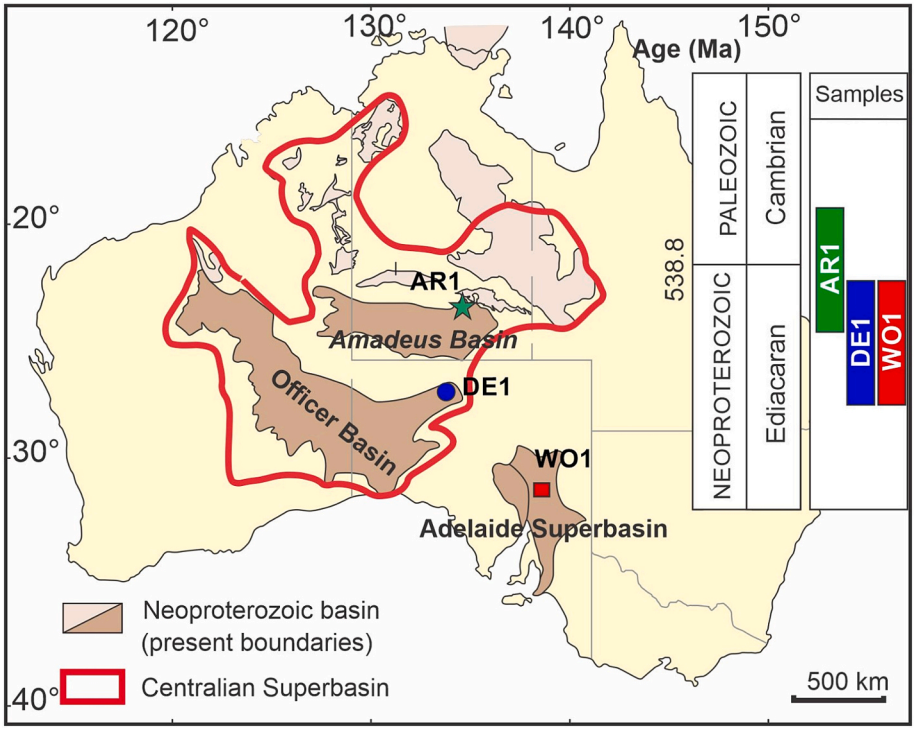

Fig. 1. Schematic view on the studied Neoproterozoic depositional systems, with the locations of glauconite-rich Ediacaran/Cambrian strata and samples analysed in this study (modified from Walter et al., 1995). Studied samples include: AR1 (Arumbera Sandstone = star symbol), DE1 (Dey Dey Mudstone = circle), and WO1 (Wonoka Formation = square).

reducing conditions (López-Quirós et al., 2020; Baldermann et al., 2025), thereby providing an archive for a direct dating of marine sediments (Löhr et al., 2024, and references therein). Glauconite in the studied Ediacaran/Cambrian strata from Australia is present in siliciclastic and mixed calcareous/siliciclastic intervals, and is present in a variety of morphologies and sizes (see Fig. 2).

2.1.1. *Arumbera sandstone*

The Arumbera Sandstone samples from the Amadeus Basin (Centralian Superbasin) were collected from outcrop, 70 km southwest from Alice Springs (Sample AR1, Fig. 1). The Arumbera Sandstone, which is part of the Pertaoorta Group and supersequence 4 (Walter et al., 1995), was deposited in the intracontinental Amadeus Basin, and mainly comprises red brown to purple-brown thinly bedded, fine and medium grained, ferruginous micaceous feldspathic sandstone, with minor pebble conglomerate and micaceous siltstone (Edgoose, 2013).

The unit is divided into two depositional successions of upward-coarsening sandstone and siltstone. Both successions were deposited in a fluvio-deltaic setting (Edgoose, 2013). The lower succession corresponds to deltas that prograded across the underlying carbonate platform of the Julie Formation, and the upper succession represents major deltaic complexes that prograded at the sub-basin scale (Mapstone and

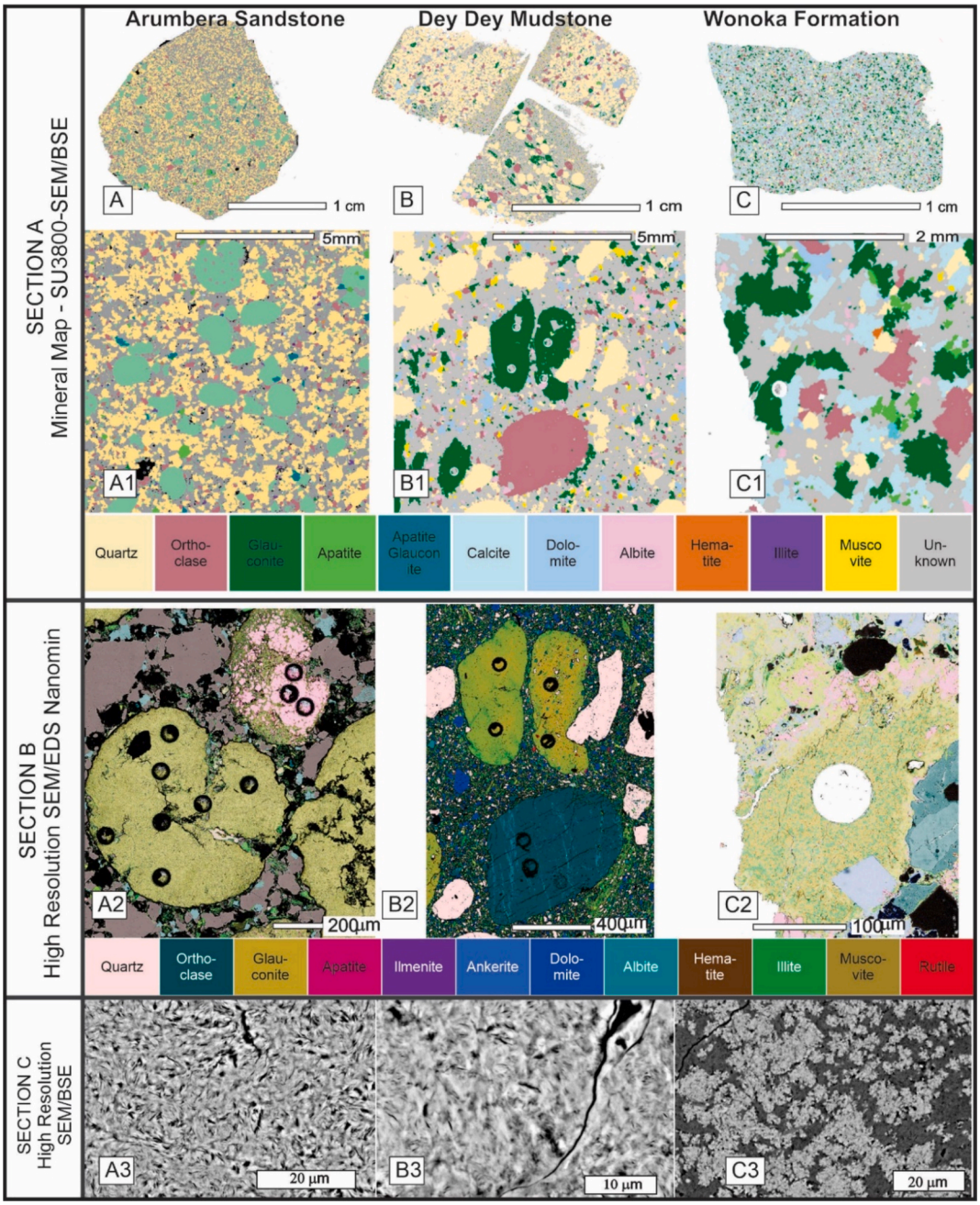

Fig. 2. Microscopic images (BSE) with mineral map (SEM/EDS) overlays illustrating occurrences of K-rich minerals (glauconite, illite, K-feldspar/orthoclase) in the studied samples from the Arumbera (AR), Dey Dey (DE), and Wonoka (WO) strata. **Section A** (Top panels): (A) a mineral map of sample AR1, with close up view (A1) on glauconite pellets; (B) a mineral map of sample DE1, with close up view (B1) on glauconite pellets and detrital orthoclase; (C) a mineral map of sample WO1, with detail view (C1) on glauconites. **Section B** (middle panels): (A2) High-resolution BSE image with Nanomin (SEM/EDS) overlay map of sample AR1; (B2) High-resolution images of glauconite sample DE1; and (C2) a sample WO1. **Section C** (bottom panels): BSE image (A3) of micro-textures in glauconite from sample AR1; (B3) glauconite from sample DE1; (C3) and glauconite from sample WO1.

McIlroy, 2006). The expected age of the Arumbera Sandstone ranges from the latest Neoproterozoic (late Ediacaran, ca. 550 Ma) to the early Cambrian (ca. 520 Ma); based on trace fossil evidence of soft-bodied Ediacaran fauna (metazoan body fossils), local geological context, and lithostratigraphic correlation (Edgoose, 2013). Note that detrital zircon U–Pb ages from the Arumbera Sandstone have a wide range, falling mainly between 1200–1000 Ma, suggesting that the primary provenance is the Musgrave Province to the south (Maidment et al., 2007; Haines et al., 2016). This provides constraints on the depositional age of this formation and glauconite-bearing strata.

2.1.2. Dey dey mudstone

The Dey Dey Mudstone, part of the Ungoolya Group, consists of two distinct units: an upper unit composed of dolomitic or calcareous siltstone, and a lower unit dominated by red-brown silty mudstone. It contains the Ediacaran Acraman impact ejecta layer, which has been dated to around 580 Ma (Webster et al., 2004; Hill et al., 2007; Rollet et al., 2024). The unit is considered to represent a prodelta and shelf environment (Zang, 1995). It is considered to be of late Ediacaran age based on its acritarch assemblage (Willman and Moczydłowska, 2008), and the presence of the Acraman ejecta layer (Morton and Drexel, 1997; Williams and Gostin, 2005).

The Dey Dey Mudstone sample DE1 (Officer Basin, Centralian Superbasin) is glauconite-rich, and was collected from Giles 1 drillhole at 497 m depth. Giles 1 is a petroleum well drilled in the largely unexplored eastern Officer Basin (Fig. 1) (Dunster, 1986). Sample DE1 is from the top of the upper unit of the Dey Dey Mudstone, just below the Karlaya Limestone, and comprises laminated calcareous siltstone and mudstone (Morton and Drexel, 1997; Willman and Moczydlowska, 2008).

2.1.3. Wonoka formation

The Wonoka Formation (Wilpena Group) samples were collected from an outcrop in the northeastern part of the Adelaide Superbasin in the Flinders Ranges (Lloyd et al. 2020). The Wonoka Formation is of upper Ediacaran age, as it hosts the arcuate tubular fossil Palaeopascichnus, identified as the oldest known Ediacaran metazoan fossil in South Australia (Haines, 2000). Additionally, this formation also preserves the late Ediacaran Shuram-Wonoka negative carbon isotope excursion (CIE), with its age constrained between ~ 570 and 560 Ma, based on purported correlations with other coeval CIEs globally (Cantine et al., 2024; Rooney et al., 2020; Williams and Schmidt, 2018).

The glauconite-rich sample WO1 was taken from Unit 7 (Haines, 2000) of the Wonoka Formation in Brachina Gorge. Based on previous observations and sedimentological studies, Unit 7 records the development of an extensive storm-dominated carbonate shelf in the central Flinders Ranges with local evidence of shallower conditions at the top of the unit (Haines, 2000).

2.2. Analytical Methods

2.2.1. Imaging and mineral mapping

Samples with glauconite-rich intervals (AR1, DE1, WO1) were selected for petrographic examination and were mounted in epoxy resin (25 mm diameter mounts), diamond polished, and carbon coated. In addition, polished thick sections (70 mm thickness) from these samples were also prepared and studied by reflected and transmitted light microscopy.

Detailed imaging and analysis of polished mounts, and thin sections were performed using a Hitachi SU3800 SEM (Scanning Electron Microscopy), equipped with a Bruker Quantax 60 mm^2 EDS (Energy Dispersive X-ray Spectroscopy) detector. Mineral mapping (SEM/EDS) was performed with a Bruker AMICS (Advanced Mineral Identification and Characterisation System), which uses BSE (Backscattered Electron) images, EDS analysis and advanced image processing to characterise and identify minerals automatically (Fig. 2.A1, 2.A2, 2.A3), for details on the above SEM/EDS and 'Nanomin' imaging techniques see also Han et al. (2022). Acquired BSE images and SEM/EDS spectra of the collected glauconite-rich samples from the Arumbera, Dey Dey and Wonoka Formations are presented in Fig. 2. Calculated mineral abundances (in weight %) in these samples, based on SEM/EDS analysis, are presented in Table 1.

2.2.2. Electron Probe Microanalysis (EPMA)

Quantitative chemical compositions (major oxides) of the studied glauconites were determined using a Cameca SX-Five Electron Probe Microanalyzer (EPMA), equipped with 5 tunable wavelength-dispersive spectrometers, and using a PeakSite v6.2 and Probe Softwares for the instrument operation and data acquisition and processing. Analysis was performed using operating conditions of 15 kV/20nA with a defocused beam of 5um.

The full list of elements analysed along with primary and interference standards are presented in Table S1 (see Supplementary Material). Oxygen was calculated by stoichiometry, assuming that all Fe was Fe2 + . Matrix corrections of Armstrong-Love/Scott φ(ρz) (Armstrong, 1988) and Henke MACs were used for data reduction.

Beam damage and alkali element migration in silicate analyses were minimized via use of a defocused electron beam, in addition to use of the Mean Atomic Number (MAN) background correction (e.g., Donovan et al., 2016; Donovan and Tingle, 1996) over traditional 2 point background interpolation. This allows single point analysis time to be greatly shortened, reducing the effects of beam damage and element migration and their subsequent impact on the quality of analysis.

In addition to this, elements that are particularly mobile (e.g., Na, F, Cl) were analysed first on the detector and the Time Dependent Intensity (TDI) correction feature of Probe for EPMA was utilized (e.g. Donovan and Rowe, 2005). Using this method, the decay of x-ray counts over time is measured and modelled to return a t = 0 intercept, and from this a concentration is calculated. The results from EPMA are shown and listed Table S2 (see Supplementary Material).

2.2.3. In situ Rb–Sr dating via LA-ICP-MS/MS

In this study we used for in situ Rb–Sr dating an Agilent 8900 QQQ ICP-MS/MS coupled to a RESOlution-LR 193 nm excimer laser ablation system at Adelaide Microscopy (following Redaa et al., 2021). In addition to Rb and Sr, the concentrations of selected trace and major elements (and their main isotopes) were simultaneously measured (^{23}Na, ^{24}Mg, ^{27}Al, ^{29}Si, ^{31}P, ^{39}K, ^{48}Ti, ^{51}V, ^{53}Cr, ^{55}Mn, ^{56}Fe, ^{65}Cu, ^{85}Y, ^{90}Zr, ^{93}Nb, ^{95}Mo, ^{139}La, ^{140}Ce, ^{141}Pr, ^{146}Nd, ^{147}Sm, ^{151}Eu, ^{157}Gd, ^{159}Tb, ^{163}Dy, ^{165}Ho, ^{166}Er, ^{169}Tm, ^{172}Yb, ^{175}Lu, ^{232}Th, ^{238}U). The operating parameters for LA-ICP MS/MS were the following: 67 μm laser spot size, 3. 5 J

Table 1
Mineralogical composition of the studied samples, from AMICS SEM-EDS mineral mapping (bld = below detection).

Mineralogy	AR1 (wt %)	DE1 (wt %)	WO1 (wt %)
Albite	0.07	4.3	1.25
Apatite	0.6	0.3	0.8
Apatite Glauconite Mix	0.7	0.04	0.23
Barite	bld	0.01	bld
Calcite	bld	0.5	80
Chlorite	0.8	bld	bld
Dolomite	bld	7	1.4
Glauconite	10.7	10.8	5
Hematite	0.2	0.01	0.04
Illite	10	bld	bld
Muscovite	bld	4	0.9
Orthoclase	6.2	10.3	2.9
Pores	10.5	0.01	bld
Quartz	60	62	6.5
Zircon	0.04	bld	bld
Total	**99.81**	**99.26**	**99.02**

cm^{-2} fluence, and 5 Hz repetition rate. The NIST-610 glass was applied as the primary reference material for drift correction and quantification of trace elements (Jochum et al., 2011).

To process the elemental and isotopic data, NIST-610 was used as the primary reference material for both $^{87}Rb/^{86}Sr$ and $^{87}Sr/^{86}Sr$, and MDC (phlogopite) as a matrix-matched secondary reference material for $^{87}Rb/^{86}Sr$ correction (Zack and Hogmalm, 2016; Redaa et al., 2022; Glorie et al., 2024). Hence, all data presented here are normalised to NIST-610 and MDC (Fig. S1, Supplementary Material). Glorie et al. (2024) report concordant ages from coexisting K-feldspar and biotite, suggesting that matrix-related effects between these phases are minimal. Given that both biotite and the MDC phlogopite standard are K-Mg-Fe-rich micas with similar matrix characteristics, we use MDC as a quality control for K-feldspar analyses.

In addition, GL-O glauconite grains with known age of 95 ± 5 Ma were also analysed (Fig. S2, Supplementary Material) (see Redaa et al., 2022; Löhr et al., 2024 and Table S3 supplementary Material). Analysis of Mica-Mg (nano-powder) was also included in each session (Hogmalm et al., 2017) (Fig. S3, Supplementary Material).

The Rb–Sr isochrons were constructed using the IsoplotR package (Vermeesch, 2018), applying the ^{87}Rb decay constant reported by Villa et al. (2015). Analysis of the GL-O grains, from three separate analytical sessions, returned ages of 94 ± 5 Ma, 93 ± 6 Ma, and 98 ± 10 Ma (Fig. S2, Supplementary Material), which are within the uncertainties of a published Rb–Sr age for 'bulk' GL-O grains (94.5 ± 4.1 Ma; Löhr et al. 2024) or the K-Ar age for a bulk GL-O of 95 ± 1.5 Ma (Redaa et al., 2022 and references therein).

2.2.4. Rare earth element analysis and data normalization

The REEs concentrations were measured simultaneously with Rb–Sr analysis for each laser spot (^{139}La, ^{140}Ce, ^{141}Pr, ^{146}Nd, ^{147}Sm, ^{151}Eu, ^{157}Gd, ^{159}Tb, ^{163}Dy, ^{165}Ho, ^{166}Er, ^{169}Tm, ^{172}Yb, ^{175}Lu). Note that the concentrations of REE for K-feldspar minerals and a pore-filling K-rich material were normalised to a chondritic meteorite standard (refer to McDonough and Sun, 1995), while the REE data acquired from glauconite grains were normalised in this study to the Post-Archean Australian Shale (Pourmand et al., 2012).

3. Results

3.1. Petrographic and mineralogical screening (optical and SEM/EDS)

3.1.1. Arumbera Sandstone

Samples collected from the Arumbera Sandstone contain glauconite grains occurring in a quartz-rich siliciclastic matrix. Quartz and orthoclase appear as 100–200 μm-sized, mostly angular, grains of detrital origin. Illite is present as inter/intragranular pore filling cement (Fig. 2-A). The glauconites are present as 250–300 μm size pellet grains. These pellets are concentrated between sandstone laminae and are oriented parallel to the lamination. Some glauconite grains are associated with apatite, showing a patchy texture with irregular patterns or mineral-phase contacts. Some of the glauconite grains show the presence of fractures, in some cases with secondary mineral infill. Sample AR1 comprises mostly quartz (~60 wt%), orthoclase (~6.2 wt%), illite (~10 wt%), and glauconite (~10.7 wt%), with minor chlorite (~0.8 wt%), apatite (~0.6 wt%), apatite-glauconite mixtures (~0.7 wt%), and associated weathered or oxidized products such as hematite (~0.2 wt%) (Fig. 2-A2, and Table 1). The intergranular porosity of this sample is estimated at ~~ca.~~ ~ 10.5 % of a ~~total volume or~~ studied area.

3.1.2. Dey Dey Mudstone

Dey Dey Mudstone samples are medium- to fine-grained glauconitic sandstones to mudstones. Quartz and orthoclase grains are well-rounded. The glauconite grains are large, typically ~ 800 to 1500 μm in diameter, presenting as oval pellets. Some of the glauconite grains show micro-inclusion, consisting mostly of feldspar, and quartz. Some of the screened glauconite grains shows patchy illitization that are mostly associated with micro-fractures and elongate cracks.

Orthoclase grains are abundant, appearing as subrounded to well-rounded grains up to 2 mm in size. Backscattered electron (BSE) imaging revealed two well-rounded grains (Supplementary Material, Fig. S4) containing quartz inclusions, with no apparent alteration. We also identified 10 subrounded grains (Supplementary Material Fig. S4) exhibiting perthitic texture and inclusions. Energy-dispersive X-ray spectroscopy (EDS) confirmed the presence of dolomite and apatite, in these grains. Based on these observations, the detrital K-feldspar grains were classified into two types: Type 1, comprising detrital K-feldspar with quartz inclusions, and Type 2, consisting of different 'K-feldspar' grains with perthitic (i.e., mixture of sodic and potassic feldspar) composition and inclusions of dolomite, and apatite.

The matrix is composed of quartz and mixture of feldspar, dolomite and illite (see also Fig. 2–B1). The sample DE1 is composed of quartz (~62 wt%), orthoclase (~10.3 wt%), dolomite (~7 wt%), albite (~4.3 wt%), muscovite (~4 wt%), and glauconite (~10.8 wt%), with minor apatite (~0.3 wt%) and calcite (~0.5 wt%) (Fig. 2 - A1, and Table 1).

3.1.3. Wonoka Formation

Samples from the Wonoka Formation contain glauconite (ranging between 60 μm and 1000 μm) in a calcite dominated matrix, and minor quartz, orthoclase, and dolomite. The glauconite grains shows curved and irregular shapes, constrained by surrounding carbonates. Quantitative mineral mapping shows that the sample WO1 is composed of calcite (~80 wt%), dolomite (~1.4 wt%), quartz (~6.5 wt%), glauconite (~5 wt%), orthoclase (~2.9 wt%), and albite (~1.25 wt%), with traces of apatite (~0.8 wt%), muscovite (~0.9 wt%) and apatite glauconite mix (~0.23 wt%) (Fig. 2 - A3, and Table 1).

3.2. Elemental composition of glauconite

The chemical composition of the major and minor elements in the studied K-rich authigenic clays/glauconite minerals are shown in Table S2. The concentration of the major oxides (SiO_2, Al_2O_3, MgO, K_2O, Fe_2O_3, CaO, Na_2O) obtained by EMP analysis of the glauconites, adjusted to $O_{10}(OH)_2$, were plotted on the compositional diagram of Fe-bearing clay phases (see Fig. 3A), following the approach of Meunier and El Albani (2007). The glauconites in samples AR1, DE1, and WO1 fall mostly within the Fe-depleted or left part of the 'glauconite field' (apart from some data from WO1 and DE1, which shows geochemical evidence for possible illitization) (see Fig. 3A). The glauconite *interlayer charge* varies between 0.6 and 0.88, with most samples falling within the glauconite field (see Fig. 3A), thus reflecting the *evolved* to *highly evolved* stage of glauconite maturation (Fig. 3B).

3.3. In situ Rb–Sr dating of glauconites

3.3.1. Arumbera sandstone glauconites

Glauconite yields a Rb–Sr isochron date of 422 ± 11 Ma (Fig. 4.A.1, n = 47, MSWD = 1.3), which is ca. 109 million years younger than the expected stratigraphic age for the Arumbera Sandstone (ca. 530 Ma) (Maidment et al., 2007; Edgoose, 2013; Haines et al., 2016). The obtained $(^{87}Sr/^{86}Sr)_0$ of 0.7235 ± 0.0069 is significantly more radiogenic than the reconstructed Sr isotope composition of the early Cambrian palaeo-seawater of ~ 0.709 (Chen et al., 2022).

3.3.2. Dey dey mudstone glauconites

The DE1 glauconite yields a Rb–Sr isochron date of 448 ± 7 Ma (Fig. 4.B.1, n = 87, MSWD = 1.6), which is ca. 120 million years younger than the expected stratigraphic age for the Dey Dey Mudstone (ca. 570 Ma) (Morton and Drexel, 1997; Williams and Gostin, 2005; Willman and Moczydłowska, 2008). The $(^{87}Sr/^{86}Sr)_0$ of 0.7145 ± 0.0027 is also more radiogenic than the Ediacaran seawater ratio of ~ 0.708 (Chen et al., 2022).

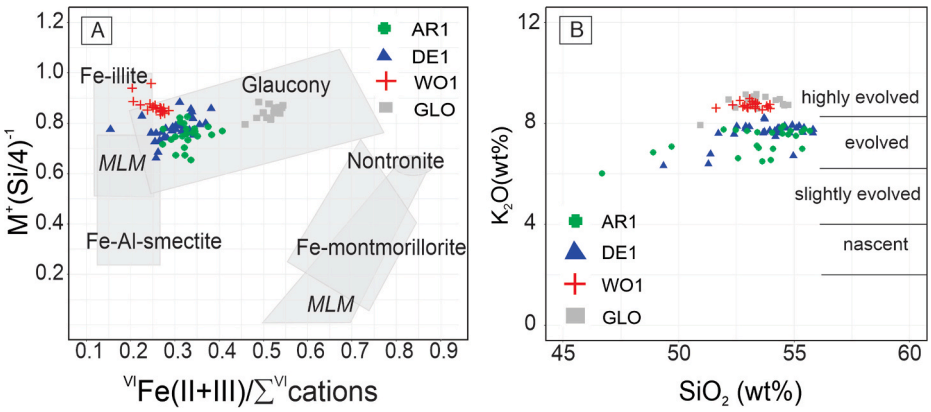

Fig. 3. (a) Compositional diagram of Fe-bearing clay mineral phases (adapted from Meunier and El Albani 2007), and (b) glauconite maturity fields assessed based on the K_2O content. Coloured symbols represent the analysed Ediacaran/Cambrian glauconites (AR1, DE1, WO1), and GL-O standards, plotted based on the acquired EMPA data (Odin and Matter, 1981) (*MLM stands for mixed-layer minerals, *M stands for interlayer charge).

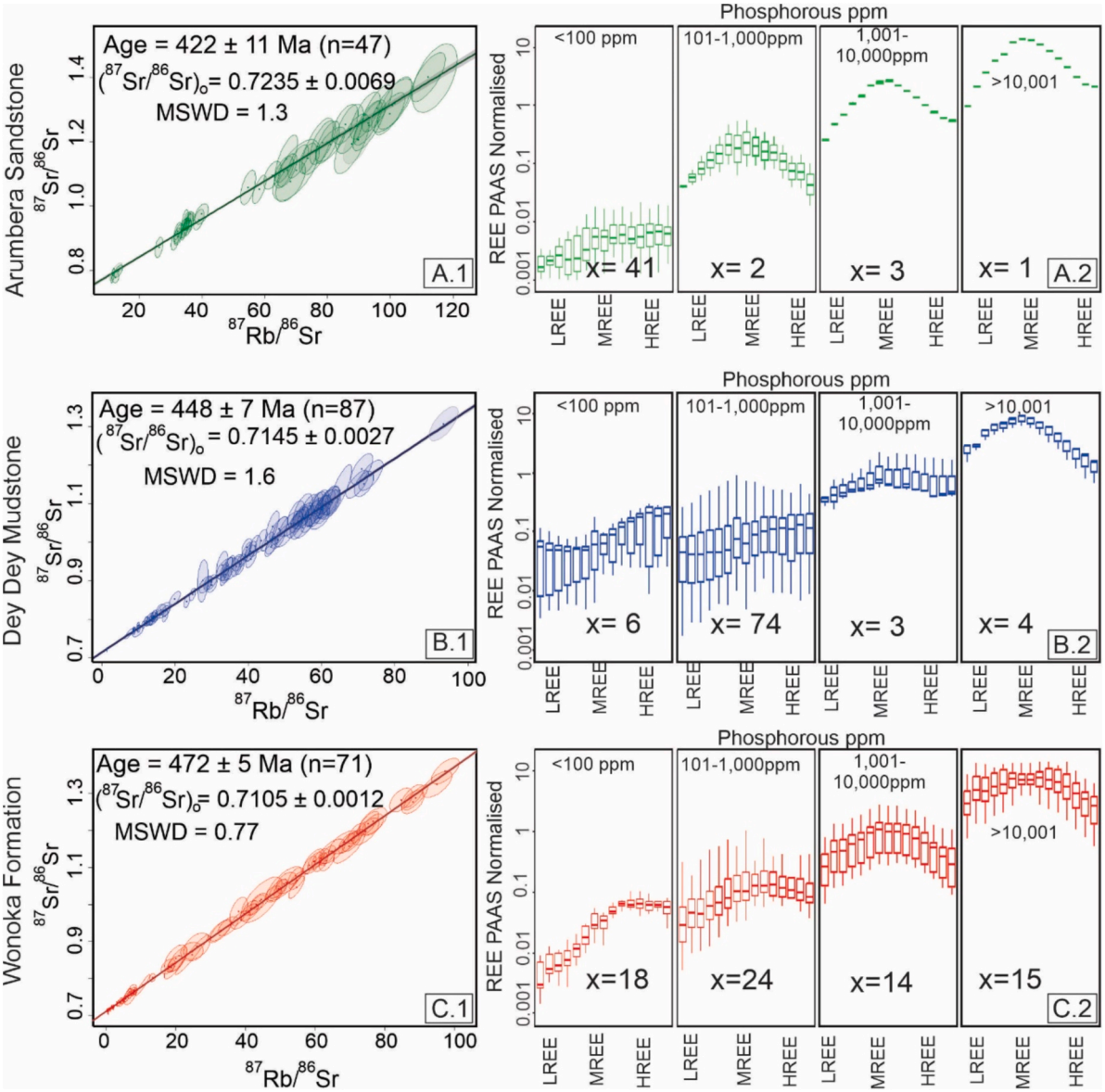

Fig. 4. Left panels: In situ $^{87}Rb/^{86}Sr$ and $^{87}Sr/^{86}Sr$ data and constructed isochrons based on the analysed glauconites grains. Right panels: Normalised REE patterns (relative to Post Archean Australian shale – PAAS), showing main trends for light (L), medium (M), and heavy (H) REE, plotted as the function of phosphorus content (ppm) in the analysed glauconites and glauconite-apatite mixtures from AR1, DE1 and WO1.

3.3.3. Wonoka formation glauconites

The WO1 glauconite yielded an age of 472 ± 5 Ma (Fig. 4.C.1, n = 71, MSWD = 0.77), which is ca. 100 million years younger than the expected stratigraphic age for the Wonoka Formation (ca. 570 Ma) (Williams & Schmidt, 2018). The $(^{87}Sr/^{86}Sr)_0$ of 0.7105 ± 0.0012 is slightly more radiogenic than the expected Ediacaran seawater ratio (Chen et al., 2022).

3.4. In situ Rb–Sr dating of detrital feldspar in the Dey Dey Mudstone

Two isochron were constructed using the petrographic classification of studied feldspars (see also Fig. S4, and Bevan et al., 2024). Type 1 detrital K-feldspar yielded an age of 1781 ± 63 Ma (Fig. 5.A, n = 11, MSWD = 3.5), whereas Type 2 grains returned an age of 1149 ± 43 Ma (Fig. 5.B, n = 26, MSWD = 1.7).

3.5. REE pattern

3.5.1. Rare earth element pattern in glauconite

Rare Earth Element (REE) concentration data acquired from glauconites and glauconite-apatite mixtures (from AR1, DE1 and WO1 samples) were normalised to the Post Archean Australian Shale (PAAS, see also Pourmand et al., 2012). Subsequently, the normalised PAAS data were categorized into 4 groups based on their phosphorus concentration, to assess the relative influence of apatite (see Fig. 4, A2, B2 and C2). The data on the left correspond to relatively 'pure' glauconites (P less than 100 ppm), while the last panel on the right represent the most apatite-rich mixtures (P > 10,000 ppm). For all studied samples, the mix phases (apatite-glauconite) show an enrichment in middle REE (MREE, Fig. 4, A2, B2, C2), while the 'pure' glauconite shows a depletion in light REE (LREE).

3.5.2. REE and in situ Rb–Sr ages of feldspar in the Arumbera Sandstone

Originally, only errorchrons for $^{87}Rb/^{86}Sr$ and $^{87}Sr/^{86}Sr$ data were constructed for feldspars (based on 36 laser spots) from the Arumbera Sandstone, Amadeus Basin (see Supplementary Material, Fig. S5.A). Consequently, the REE patterns in these feldspars were also analysed (Table S4). A total of 19 spot analyses exhibited an Eu anomaly greater than 10, but this subset still yielded errorchrons, but a correlation was identified between these data and P concentration (ppm) (see Supplementary Material, Fig. S5.C). Hence, the data were filtered based on their P concentrations and specifically using P concentrations > 300 ppm which yielded an isochron for Rb–Sr feldspar data with an age of 1565 Ma ± 48 Ma (n = 11, MSWD = 1.9), and $(^{87}Sr/^{86}Sr)_0$ of 0.7277 ± 0.0046 (see Fig. 6.B).

Based on the chondrite-normalised REE patterns, and the abovementioned criteria, we also identified a group of K-rich silicate minerals present within intergranular/pore spaces (in the sample AR1), which in turn exhibit a negative Eu/Eu* anomalies. Closer inspection and imaging (Fig. S6, Supplementary Material) confirmed that this group represents a complex mixture of 'pore filling' K-rich silicates, including fine-grain illite/glauconite, micas, and K-feldspar mixed phases, which yielded an apparent isochron (or a 'mixing line') with a slope equivalent to an age of 530 ± 67 Ma (n = 15, MSWD = 2.1), and a $(^{87}Sr/^{86}Sr)_0$ of 0.7163 ± 0.0093 (Fig. 7.B). Interestingly, this 'age' overlaps (within uncertainty) with the expected depositional age of the Arumbera Sandstone.

4. Discussion

4.1. Glauconite maturation vs. Illitization

Glauconite pellets in all three studied samples (AR1, DE1, WO1) show evidence of alteration or illitization (i.e., conversion to Fe-rich illite), compared to relatively pristine or 'pure' glauconite phases (the latter represented by GLO standard, see also data in Fig. 3). Such alteration phenomena of studied grains are also supported by the occurrence of fractures containing secondary infill observed in glauconites from the sample AR1 (Arumbera Sandstone), and also by complex, angular and irregular shapes of the glauconites from the sample WO1 (Wonoka Formation). The subangular morphology of glauconite in sample WO1 may result from later stage alteration and recrystallization in contact with the surrounding carbonates (Rafiei et al., 2023).

Diagenetic alteration or transformation of glauconite into illite (accompanied by Fe loss and mobilization of other cations) is thought to be mainly controlled by the composition of diagenetic fluid, temperature, and burial history (Bansal et al, 2019; Guimaraes et al, 2000). Typically, the glauconitization process occurs at low temperatures within a sediment–seawater interface, and involves the gradual maturation of Fe-smectite into glauconite through mixed layered 'glauconite-smectite' step, associated with a progressive uptake and incorporation of K and Fe cations into a glauconite (at the expense of Al^{3+}, which is being gradually released or replaced by Fe^{3+}) (Odin & Dodson, 1982; Meunier & El Albani, 2007). Such maturation process typically occurs under near-equilibrium chemical conditions with respect to ambient seawater or seawater-derived pore fluid(s) within a confined, partially reducing microenvironments in a marine sediment. The degree of glauconite maturity determined for the studied late Ediacaran/early Cambrian samples from Australia can be defined as 'evolved' (samples AR1 and DE1) to 'highly evolved' (WO1) (Fig. 3), according to the scheme of Odin and Mather (1981).

Previous studies showed that glauconite tend to chemically

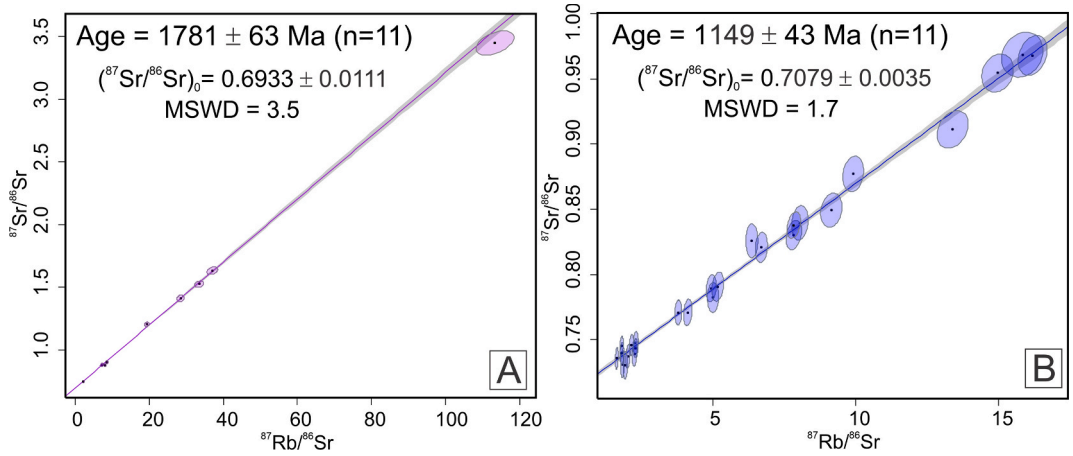

Fig. 5. In situ $^{87}Rb/^{86}Sr$ and $^{87}Sr/^{86}Sr$ data and constructed isochrons based on the analysed detrital K-feldspar grains from sample DE1, Type 1 on the left panel, and Type 2 on the right panel.

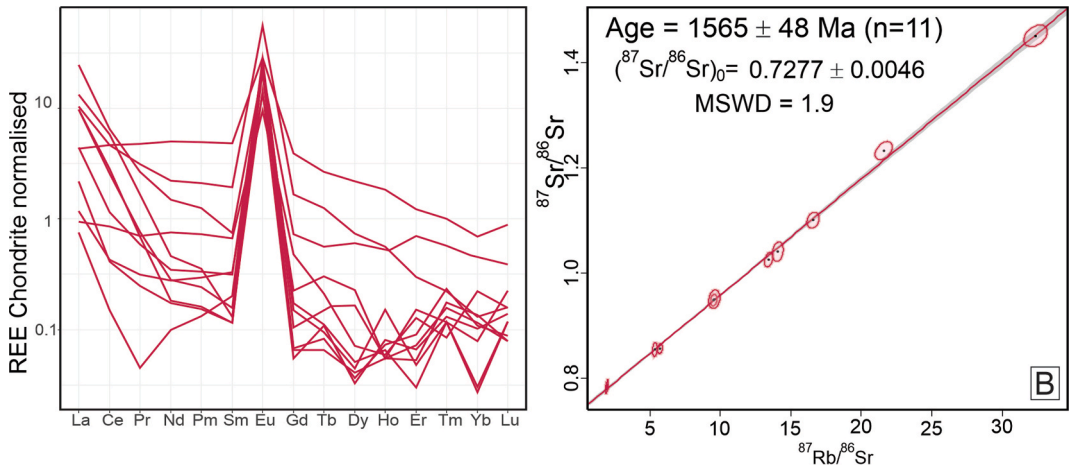

Fig. 6. (left) Chondrite normalised REE trends for detrital orthoclase/K-feldspar grains in the Arumbera Sandstone – sample AR1; (right) In situ Rb–Sr isochron and an age constructed from K-feldspar data (with Eu/Eu* >10, and P > 300 ppm) acquired from a sample AR1.

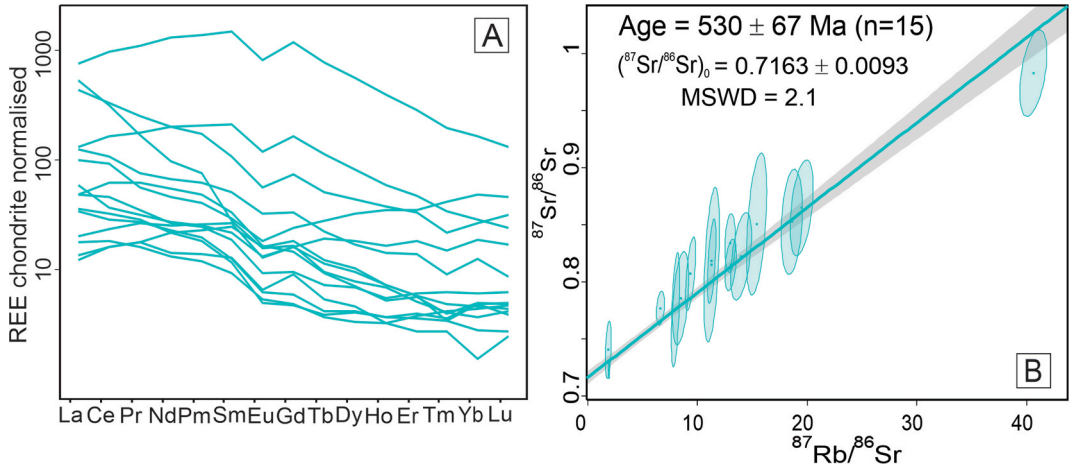

Fig. 7. (a) REE patterns of pore filling K-rich material phases in pore space of the sample AR1 (Arumbera Sandstone). (b) in situ Rb–Sr isochron and age of the pore filling K-rich material from the sample AR 1, which showed a negative Eu anomaly and enrichments in HREE and MREE relative to chondrite (see also Fig. S.6).

equilibrate with ambient porewaters or diagenetic fluids (Ireland et al, 1983; Clauer et al., 1992; Chaudhuri and Clauer, 1993; Rafiei et al., 2023). Keppens & Pasteels (1982) argued that mica-type minerals, like glauconite, with interlayer-associated cations, such as K^+ (and by interference Rb^+), are susceptible to ion exchange reactions with the diagenetic fluids. Chaudhuri and Clauer (1993) studied the K and Rb content of formation waters in sedimentary basins hosting glauconites, and they discovered that the K and Rb contents of a great majority of oil-field waters are depleted in K, but enriched in Rb, relative to evaporite brines. The K and Rb characteristics of many formation waters and/or late diagenetic (basinal) fluids are thus linked to complex process of illitization, associated with deep burial diagenesis of marine sediments (Chaudhuri and Clauer, 1993).

Accordingly, the evolution of glauconite chemistry through geological time is significantly controlled by specific diagenetic, burial history and related alteration history and post-depositional processes (Ireland 1983, Cecil and Ducea, 2011; Drits et al, 2013; Środoń et al., 2023). In Fig. 3.A, the Ediacaran/Cambrian glauconites from this study that have a rather low Fe content, thus indicate some degree of Fe loss or illitization likely due to such burial and diagenetic alteration and recrystallization (see also Strickler & Ferrell, 1990; Guimaraes et al., 2000).

In terms of geochronology, Cecil and Ducea (2011) showed that Palaeozoic glauconites yielded K–Ca ages that are systematically younger than the respective Rb–Sr ages, and both tend to be younger than the expected depositional ages. This observation suggests that these two geochronometers in glauconites tend to get reset under different diagenetic/burial conditions, or alternatively they recorded two different diagenetic or resetting events after the deposition (Cecil and Ducea, 2011).

Regardless, these results indicate that the K–Ca system is potentially useful as a low-temperature thermochronometer with a closure temperature of < 100 °C (in the range of the apatite fission track (AFT) sensitivity), while the Rb–Sr system in glauconite seems to be more robust, yet also prone to post-depositional resetting at higher temperatures or elevated mineral-fluid interactions. Overall, the observations by Cecil and Ducea (2011) are consistent with the partly reset or 'rejuvenated' Rb–Sr ages analysed in this study from the Ediacaran/Cambrian glauconites from Australia. For example, the glauconites from the late Ediacaran Dey Dey Mudstone (DE1), yielded a Rb–Sr isochron age of 448 ± 7 Ma, while the published AFT from the same drillhole indicate a maximum burial or reset temperature of ca. 95 to 100 °C, occurring after the deposition (between ~ 400 Ma and ~ 250 Ma), based on AFT data from the overlying Tanana Formation, and the underlying the Meramangye Formation (Tingate & Duddy, 2002). In summary, all glauconite samples from the Centralian and Adelaide Superbasins analysed in this study (samples AR1, DE1, and WO1) returned systematically younger ages compared to the expected depositional ages (see Fig. 8). However, these 'rejuvenated' glauconite Rb–Sr ages seem to overlap

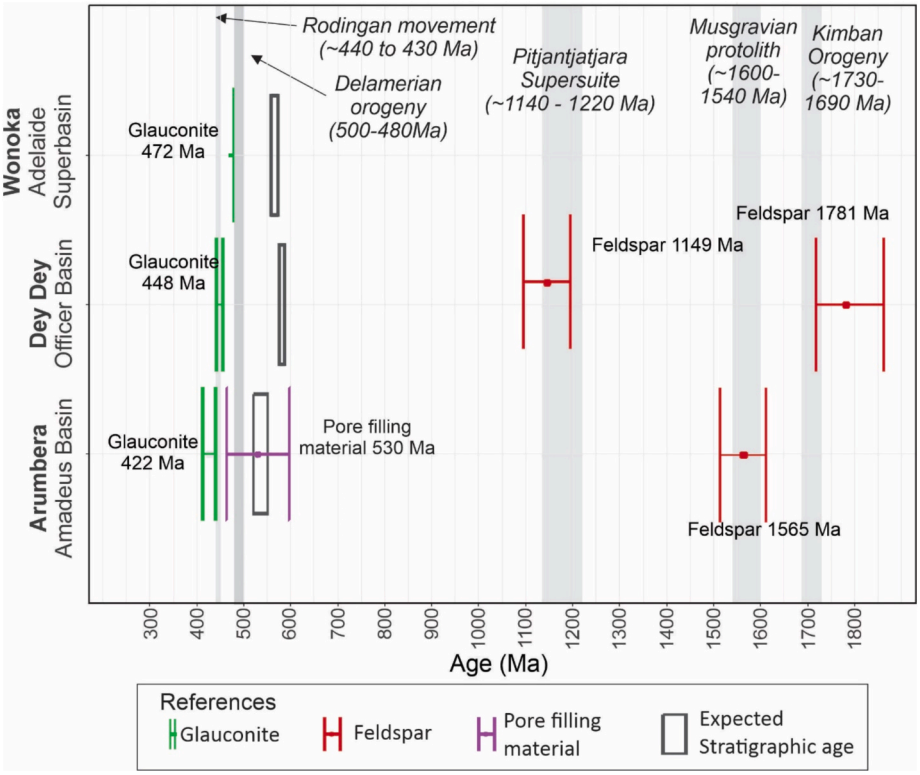

Fig. 8. A summary diagram showing the acquired ages from in situ Rb–Sr dating of the studied Ediacaran/Cambrian glauconites from Australia (green), detrital feldspars (red), and pore filling K-rich material (purple); which are plotted along with the expected (i) depositional ages (open rectangles), and (ii) major tectonic and orogenic events (grey rectangles) occurring in the central Australia (Centralian and Adelaide Superbasins), including Rodingan Event, Delamerian Orogeny, Pitjantjatjara Supersuite and Kimban Orogeny.

with the timing of the main tectonic or orogenic events that occurred in the region (e.g., Alice Springs Orogeny/Rodingan Movements, and Delamerian Orogeny), (Fig. 8). The Arumbera Sandstone (AR1, Amadeus Basin) yielded an age of 422 ± 11 Ma, likely reset by the Rodingan Event or early Alice Springs Orogeny-related cooling. The Dey Dey Mudstone (DE1, Officer Basin) showed a 448 ± 7 Ma age, significantly younger than its depositional age, suggesting partial resetting during the onset of the Alice Springs Orogeny, with later thermal events insufficient to alter the system—implying a closure temperature above 100 °C. The Wonoka Formation (WO1, Adelaide Superbasin) produced a 472 ± 5 Ma age, interpreted as reflecting post-Delamerian thermal overprinting during the Ordovician (Fig. 8).

We propose that higher temperatures and enhanced fluid-rock interactions driven by the above orogenic events, might have caused (i) thermal/chemical diffusion and mobilisation of Rb and Sr within the studied glauconites, and (ii) increased major ions exchange (K^+, Fe^{3+}, Al^{3+}, etc) between glauconite and diagenetic/burial fluid(s), resulting the observed partial illitization (Fe loss) and the 'rejuvenated' Rb–Sr ages.

4.2. Interpretation of REE patterns in the Ediacaran/Cambrian glauconites

The REE data collected from 'pure' glauconite in samples AR1, DE1, and WO1, all show a depletion in LREE (see Fig. 4). In contrast, our REE data from glauconite-apatite mixtures (P greater than 10,000 ppm) show enrichments in MREE.

Byrne et al., (1996) showed that phosphate coprecipitation leads to middle REE (MREE) depletion of seawater. Consequently, the REE signatures of various phosphatic minerals—including authigenic (Kidder and Eddy-Dilek, 1994), biogenic (Williams et al., 1997), and igneous (El-Haddad and Ahmed, 1991) types—typically exhibit marked MREE enrichments when normalized to shale. Such "hat-shaped" patterns (observed in the mixtures) may be linked to a marine pore-water REE chemistry or composition from which the early diagenetic apatite has formed. The enrichment in MREE in marine pore fluids is presumably due to reductive dissolution of ambient Fe-oxy/hydroxides within a sediment, which tend to release MREE into marine pore fluids, causing the 'hat-shaped' REE pattern. The latter can then be incorporated into early diagenetic minerals, such as apatite and/or marine authigenic clays, as observed in our apatite-glauconite mix REE data and patterns (Fig. 4), (see also Chen et al., 2015; Zhang et al., 2016; Smrzka et al. 2019).

4.2.1. Detrital feldspar Rb–Sr ages from Dey Dey Mudstone

Rb–Sr dating of the two petrographically distinct feldspar groups revealed two separate ages: 1781 ± 63 Ma, and 1149 ± 42 Ma. These ages agree with known sources of igneous/metamorphic rocks or terrains in central Australia from which these detrital feldspars might have been derived. Briefly, the Rb–Sr feldspar ages of the older grains (Type 1, Fig. 5) coincide with the Kimban Orogeny (1730–1690 Ma; see also Fig. 8), which is well documented in the Gawler Craton, southeast of the Officer Basin (Wilson, 2021; and references therein). In contrast, the younger Rb–Sr ages of the Type 2 feldspar grains (ca. 1149 Ma) coincide with the timing of the Musgrave Orogeny magmatism and related igneous rocks (ca. 1140–1220 Ma) (Glorie et al., 2017), which crop out north of the Officer Basin.

4.2.2. Detrital feldspar REE patterns and Rb–Sr ages from Arumbera Sandstone

For igneous/metamorphic feldspars and their detrital products, REE patterns have been used extensively to support various petrogenetic models and possible sources, where the REE patterns or distributions are controlled by multiple factors and high-temperature processes, such as

partial melting, fractional crystallisation, mobilisation due to metamorphism, fluid-rock interactions, etc (Schilling and Winchester, 1967; Gast 1968; Henderson, 1984; Kontonikas-Charos et al., 2017), thus providing additional 'fingerprints' via REEs to constrain the provenance of detrital feldspars in depositional systems.

The chondrite-normalised REE concentration and patterns from the detrital K-feldspar from the Amadeus Basin, hosted in the Arumbera Sandstone (sample AR1), were calculated. K-feldspars that have positive Eu/Eu* anomalies and elevated P contents (>300 ppm) yielded an in situ Rb–Sr age of 1565 ± 48 Ma. This overlaps with the age of igneous/metamorphic rocks and gneisses from the Musgrave Province (1600–1540 Ma; Edgoose et al., 2004; Haines et al., 2016), which is located to the south from the Amadeus Basin, thus providing a likely source of these detrital feldspars in the Arumbera Sandstone. Previous studies on detrital zircon sources suggest that the provenance of the Arumbera Sandstone and its lateral equivalents is predominantly linked to the Musgrave Province, associated with the Petermann Orogeny (Haines et al., 2016). This interpretation agrees with the origin and possible sources (based on the Rb–Sr age constraints) for the detrital feldspar grains analysed in this study. However, due to the generally low concentrations of REEs in feldspars, the potential influence and impact of non-feldspatic micro-inclusions within the studied grains cannot be ruled out, and more systematic studies are needed to carefully avoid and quantify such effects for more robust interpretations of coupled REEs patterns and Rb–Sr ages in detrital feldspars for provenance studies.

5. Conclusions

This study demonstrates the potential of novel in situ Rb–Sr geochronology, coupled with REE analysis, to constrain both the post-depositional history of marine glauconite-bearing sedimentary rocks and the provenance of detrital K-feldspar grains in late Proterozoic to early Paleozoic sedimentary archives of the Australian basins.

Results from the Centralian (Amadeus, Officer Basins) and Adelaide Superbasins (Flinders Ranges) show that the studied late Ediacaran/early Cambrian glauconites yielded systematically younger or reset in situ Rb–Sr ages. These ages correlate with petrographic and geochemical evidence of post-depositional diagenetic alteration, including partial illitization (transformation of glauconite to Fe-rich illite). These younger Rb–Sr ages likely reflect rejuvenation events linked to major tectonothermal overprints, such as the Alice Springs and Delamerian Orogenies (Foden et al., 2006; Foden et al., 2020).

REE data further support this interpretation, showing patterns indicative of mixing between 'pure' glauconite and early diagenetic apatite micro-inclusions, resulting in characteristic MREE-enriched, 'hat-shaped' patterns—consistent with REE signatures of marine pore fluids at the iron redoxcline.

Moreover, the integration of REE patterns coupled with microscopic (BSE, SEM-EDS) and petrographic analyses of detrital K-feldspar grains provides an effective approach to distinguish between grain populations, which in turn enables the identification of distinct Rb–Sr ages in detrital grains.

Together, these findings show that laser-based Rb–Sr and REE analyses of both authigenic (glauconite) and detrital (orthoclase) K-bearing minerals offer a valuable approach for interpreting the diagenetic evolution and sedimentary provenance of ancient siliciclastic systems. This technique complements traditional U–Pb zircon dating and expands the geochronological toolkit for reconstructing the complex histories of Proterozoic and Paleozoic basins.

CRediT authorship contribution statement

Cecilia Loyola: Writing – original draft, Investigation, Formal analysis, Data curation. **Juraj Farkaš:** Visualization, Validation, Supervision, Resources, Project administration, Methodology, Investigation, Funding acquisition, Conceptualization. **Alan S. Collins:** Writing – review & editing, Resources, Project administration, Methodology, Investigation, Funding acquisition. **Sarah E. Gilbert:** Writing – review & editing, Methodology, Investigation, Formal analysis, Data curation. **Charles Verdel:** Investigation, Data curation. **Stefan C. Löhr:** Writing – review & editing, Methodology, Investigation, Data curation. **Glenn A. Brock:** Writing – review & editing, Resources, Investigation. **Graham A. Shields:** Writing – review & editing, Investigation. **Andre Baldermann:** Writing – review & editing, Data curation. **Ahmad Redaa:** Writing – review & editing, Data curation. **Morgan Blades:** Writing – review & editing, Data curation. **Darwinaji Subarkah:** Writing – review & editing, Data curation. **Caleb Bishop:** Writing – review & editing, Resources. **Sarah M. Giles:** Writing – review & editing, Data curation. **Nicholas Christie-Blick:** Writing – review & editing. **Peter W. Haines:** Writing – review & editing, Resources.

Declaration of competing interest

The authors declare that they have no known competing financial interests or personal relationships that could have appeared to influence the work reported in this paper.

Acknowledgments

This study was funded via the Australian Research Council - ARC Discovery Project (DP210100462) titled 'Glauconite: Archive Recording Timing and Triggers of Cambrian Radiation', and ARC Linkage Project (LP210200822) titled 'Novel Isotope Techniques to Explore the Centralian Superbasin, Australia'. In addition, a financial support for the industry-academia PhD scholarship (iPhD) to Cecilia Loyola via the University of Adelaide and Santos Ltd is also greatly acknowledged. Peter Haines publishes with the permission of the Executive Director of the Geological Survey of Western Australia. The work has been supported by the Mineral Exploration Cooperative Research Centre whose activities are funded by the Australian Government's Cooperative Research Centre Program. The authors acknowledge the instruments and expertise of Microscopy Australia (ROR: 042mm0k03) at Adelaide Microscopy, University of Adelaide, enabled by NCRIS, university, and state government support. Finally, we would also like to acknowledge the time and constructive comments from two reviewers, as well as the excellent and timely editorial handling.

Appendix A. Supplementary data

Supplementary data to this article can be found online at https://doi.org/10.1016/j.precamres.2025.107851.

Data availability

Data will be made available on request.

References

Armstrong, J.T., 1988. Quantitative analysis of silicate and oxide minerals: Comparison of Monte Carlo, ZAF, and φ(ρz) procedures. In: Newbury, D.E. (Ed.), *Microbeam Analysis*. San Fransisco Press, pp. 239–246.

Baldermann, A., Banerjee, S., Löhr, S.C., Rudmin, M., Warr, L.N., Chakraborty, A., 2025. Exploring reverse silicate weathering across geological time: a review. Clay Miner. 1–93.

Bansal, U., Banerjee, S., Pande, K., Ruidas, D.K., 2019. Unusual seawater composition of the late cretaceous tethys imprinted in glauconite of Narmada basin, central India. Geol. Mag. 157 (2), 233–247. https://doi.org/10.1017/s0016756819000621.

Bevan, D., Stubbs, D., Coath, C.D., Lewis, J., Elliott, T., 2024. Detrital K-feldspar as a novel archive of continental crustal evolution using coupled in situ Rb Sr dating and Pb isotope analysis. Chem. Geol. 670, 122379. https://doi.org/10.1016/j.chemgeo.2024.122379.

Byrne, R.H., Liu, X., Schijf, J., 1996. The influence of phosphate coprecipitation on rare earth distributions in natural waters. Geochim. Cosmochim. Acta 60 (17), 3341–3346.

Cantine, M.D., Rooney, A.D., Knoll, A.H., Gómez-Pérez, I., al Baloushi, B., Bergmann, K. D., 2024. Chronology of Ediacaran sedimentary and biogeochemical shifts along eastern gondwanan margins. Commun. Earth Environ. 5 (1), 520.
Cawood, P.A., Hawkesworth, C.J., Dhuime, B., 2012. Detrital zircon record and tectonic setting. Geology 40 (10), 875–878. https://doi.org/10.1130/G32945.1.
Cecil, M.R., Ducea, M.N., 2011. K–Ca ages of authigenic sediments: examples from paleozoic glauconite and applications to low-temperature thermochronometry. Int. J. Earth Sci. 100 (8), 1783–1790. https://doi.org/10.1007/s00531-010-0618-y.
Chaudhuri, S., Clauer, N., 1993. Strontium isotopic compositions and potassium and rubidium contents of formation waters in sedimentary basins: clues to the origin of the solutes. Geochimica et Cosmochimica Acta 57 (2), 429–437. https://doi.org/10.1016/0016-7037(93)90441-X.
Chen, J., Algeo, T.J., Zhao, L., Chen, Z.-Q., Cao, L., Zhang, L., Li, Y., 2015. Diagenetic uptake of rare earth elements by bioapatite, with an example from lower Triassic conodonts of South China. Earth Sci. Rev. 149, 181–202. https://doi.org/10.1016/j.earscirev.2015.01.013.
Chen, X., Zhou, Y., Shields, G.A., 2022. Progress towards an improved precambrian seawater Sr/Sr curve. Earth Sci. Rev. 224, 103869. https://doi.org/10.1016/j.earscirev.2021.103869.
Clauer, N., Keppens, E., Stille, P., 1992. Sr isotopic constraints on the process of glauconitization. Geology 20 (2), 133–136. https://doi.org/10.1130/0091-7613(1992)020<0133:SICOTP>2.3.CO;2.
Collett, S., 2025. Detrital zircon tales between the rodinia and Pangaea supercontinents; exploring connections between avalonia, cadomia and Central Asia. J. Geol. Soc. London 182 (1), jgs2024-2026. https://doi.org/10.1144/jgs2024-026.
Cox, G.M., Isakson, V., Hoffman, P.F., Gernon, T.M., Schmitz, M.D., Shahin, S., Collins, A. S., Preiss, W., Blades, M.L., Mitchell, R.N., 2018. South Australian U-Pb zircon (CA-ID-TIMS) age supports globally synchronous Sturtian deglaciation. Precambr. Res. 315, 257–263. https://doi.org/10.1016/j.precamres.2018.07.007.
Donovan, J.J., Rowe, M., 2005. Techniques for improving quantitative analysis of mineral glasses. Geochim. Cosmochim. Acta 69 (10), A589.
Donovan, J.J., Tingle, T.N., 1996. An improved mean atomic number background correction for quantitative microanalysis. Microsc. Microanal. 2 (1), 1–7. https://doi.org/10.1017/S1431927696210013.
Donovan, J.J., Singer, J.W., Armstrong, J.T., 2016. A new EPMA method for fast trace element analysis in simple matrices. Am. Mineral. 101 (8), 1839–1853. https://doi.org/10.2138/am-2016-5628.
Drits, V.A., Sakharov, B.A., Ivanovskaya, T.A., Pokrovskaya, E.V., 2013. Crystal-chemical microheterogeneity of precambrian globular dioctahedral mica minerals. Lithol. Min. Resour. 48 (6), 489–513. https://doi.org/10.1134/S0024490213060035.
Drost, K., Chew, D., Petrus, J.A., Scholze, F., Woodhead, J.D., Schneider, J.W., Harper, D. A.T., 2018. An image mapping approach to U–Pb LA–ICP–MS carbonate dating and applications to direct dating of carbonate sedimentation. Geochem. Geophys. Geosyst. 19 (12), 4631–4648. https://doi.org/10.1029/2018GC007850.
Dunster, J. (1986). Giles-1 well completion report, PEL 23, northeastern Officer Basin, for Comalco Aluminium Ltd. South Australia. *Department of Mines and Energy*. Open file Envelope, 6547.
Edgoose, C. (2013). Chapter 23: Amadeus Basin. In A. M, M. TJ (Eds.), *Geology and Mineral Resources of the Northern Territory* (Vol. 5, pp. 23)., NTGS Special Publication.
Edgoose, C. J., Scrimgeour, I. R., Close, D. F. (2004). *Geology of the Musgrave Block, Northern Territory*. Northern Territory Geological Survey, Report 15. https://geoscience.nt.gov.au/gemis/ntgsjspui/handle/1/81551.
El-Haddad, M.A., Ahmed, E.A., 1991. Facies control on the distribution of some trace and rare earth elements in egyptian phosphorites. J. Afr. Earth Sci. 12 (3), 429–435.
Eriksson, P.G., Condie, K.C., Tirsgaard, H., Mueller, W., Altermann, W., Miall, A.D., Aspler, L.B., Catuneanu, O., Chiarenzelli, J.R., 1998. Precambrian clastic sedimentation systems. Sed. Geol. 120 (1–4), 5–53. https://doi.org/10.1016/S0037-0738(98)00026-8.
Foden, J., Elburg, M., Turner, S., Clark, C., Blades, M.L., Cox, G., Collins, A.S., Wolff, K., George, C., 2020. Cambro-Ordovician magmatism in the Delamerian orogeny: implications for tectonic development of the southern gondwanan margin. Gondw. Res. 81, 490–521. https://doi.org/10.1016/j.gr.2019.12.006.
Foden, J., Elburg, M.A., Dougherty-Page, J., Burtt, A., 2006. The timing and duration of the Delamerian orogeny: correlation with the ross orogen and implications for Gondwana assembly. J. Geol. 114 (2), 189–210. https://doi.org/10.1086/499570.
Gast, P.W., 1968. Trace element fractionation and the origin of tholeiitic and alkaline magma types. Geochim. Cosmochim. Acta 32 (10), 1057–1086. https://doi.org/10.1016/0016-7037(68)90108-7.
Gehrels, G., 2014. Detrital zircon U–Pb geochronology applied to tectonics. Annu. Rev. Earth Planet. Sci. 42 (1), 127–149. https://doi.org/10.1146/annurev-earth-050212-124012.
Giresse, P., 2022. Quaternary glauconitization on gulf of Guinea, glauconite factory: overview of and new data on tropical atlantic continental shelves and deep slopes. Minerals 12 (7), 908. https://doi.org/10.3390/min12070908.
Glorie, S., Agostino, K., Dutch, R., Pawley, M., Hall, J., Danišík, M., Evans, N.J., Collins, A.S., 2017. Thermal history and differential exhumation across the eastern Musgrave Province, South Australia: insights from low-temperature thermochronology. Tectonophysics 703–704, 23–41. https://doi.org/10.1016/j.tecto.2017.03.003.
Glorie, S., Gilbert, S.E., Hand, M., Lloyd, J.C., 2024. Calibration methods for laser ablation Rb–Sr geochronology: comparisons and recommendation based on NIST glass and natural reference materials. Geochronology 6 (1), 21–36. https://doi.org/10.5194/gchron-6-21-2024.
Gorojovsky, L., Alard, O., 2020. Optimisation of laser and mass spectrometer parameters for the in-situ analysis of Rb/Sr ratios by LA-ICP-MS/MS. J. Anal. At. Spectrom 35 (10), 2322–2336. https://doi.org/10.1039/d0ja00308e.
Gray, A.L., 1985. Solid sample introduction by laser ablation for inductively coupled plasma source mass spectrometry. Analyst 110 (5), 551–556. https://doi.org/10.1039/AN9851000551.
Guimaraes, E.M., Velde, B., Hillier, S., 2000. Diagenetic/anchimetamorphic changes on the proterozoic glauconite and glaucony from the Paranoa group mid-western Brazil. Braz. J. Geol. 30 (3), 363–366.
Haines, P.W., 2000. Problematic fossils in the late neoproterozoic wonoka formation, South Australia. Precambr. Res. 100 (1–3), 97–108. https://doi.org/10.1016/s0301-9268(99)00070-4.
Haines, P.W., Kirkland, C.L., Wingate, M.T.D., Allen, H., Belousova, E.A., Gréau, Y., 2016. Tracking sediment dispersal during orogenesis: a zircon age and hf isotope study from the western Amadeus Basin, Australia. Gondw. Res. 37, 324–347. https://doi.org/10.1016/j.gr.2015.08.011.
Han, S., Löhr, S., Abbott, A., Baldermann, A., Farkaš, J., McMahon, W., Milliken, K., Rafiei, M., Wheeler, C., Owen, M., 2022. Earth system science applications of next generation SEM-EDS automated mineral mapping. Front. Earth Sci. 10, 956912. https://doi.org/10.3389/feart.2022.956912.
Henderson, P. (1984). General geochemical properties and abundances of the rare earth elements. In *Developments in geochemistry* (Vol. 2, pp. 1–32). Elsevier. DOI: 10.1016/B978-0-444-42148-7.50006-X.
Hill, A.C., Haines, P.W., Grey, K., Willman, S., 2007. New records of Ediacaran acraman ejecta in drillholes from the Stuart shelf and Officer Basin, South Australia. Meteorit. Planet. Sci. 42 (11), 1883–1891. https://doi.org/10.1111/j.1945-5100.2007.tb00547.x.
Hogmalm, K.J., Zack, T., Karlsson, A.K.O., Sjöqvist, A.S., Garbe-Schönberg, D., 2017. In situ Rb–Sr and K–Ca dating by LA-ICP-MS/MS: an evaluation of N_2O and SF_6 as reaction gases. J. Anal. At. Spectrom 32 (2), 305–313. https://doi.org/10.1039/C6JA00362A.
Holland, H.D., 2006. The oxygenation of the atmosphere and oceans. Philos. Trans. R. Soc., B 361 (1470), 903–915. https://doi.org/10.1098/rstb.2006.1838.
Ireland, B.J., Curtis, C.D., Whiteman, J.A., 1983. Compositional variation within some glauconites and illites and implications for their stability and origins. Sedimentology 30 (6), 769–786. https://doi.org/10.1111/j.1365-3091.1983.tb00710.x.
Jochum, K.P., Weis, U., Stoll, B., Kuzmin, D., Yang, Q., Raczek, I., Jacob, D.E., Stracke, A., Birbaum, K., Frick, D.A., 2011. Determination of reference values for NIST SRM 610–617 glasses following ISO guidelines. Geostand. Geoanal. Res. 35 (4), 397–429. https://doi.org/10.1111/j.1751-908X.2011.00120.x.
Keppens, E., Pasteels, P. (1982). Comment on the paper: "A test of the reliability of the Rb–Sr dates for selected glauconite morphologies of the upper Cretaceous (Navesink Formation) of New Jersey," by R.L. Montag and D.E. Seidemann. *Earth and Planetary Science Letters*, 58(3), 439–441. DOI: 10.1016/0012-821X(82)90092-9.
Kidder, D.L., Eddy-Dilek, C.A., 1994. Rare-earth element variation in phosphate nodules from midcontinent pennsylvanian cyclothems. J. Sediment. Res. 64 (3a), 584–592.
Knoll, A. H. (2015). *Life on a young planet: The first three billion years of evolution on Earth* (Updated ed.). Princeton University Press.
Kontonikas-Charos, A., Ciobanu, C.L., Cook, N.J., Ehrig, K., Krneta, S., Kamenetsky, V.S., 2017. Rare earth element geochemistry of feldspars: examples from fe-oxide cu-au systems in the olympic cu-au province, South Australia. Mineral. Petrol. 112 (2), 145–172. https://doi.org/10.1007/s00710-017-0533-z.
Lloyd, J.C., Blades, M.L., Counts, J.W., Collins, A.S., Amos, K.J., Wade, B.P., Hall, J.W., Hore, S., Ball, A.L., Shahin, S., 2020. Neoproterozoic geochronology and provenance of the Adelaide superbasin. Precambr. Res. 350, 105849. https://doi.org/10.1016/j.precamres.2020.105849.
Löhr, S., Khazaie, E., Farkaš, J., Baldermann, A., Gilbert, S., Maasl, R., Subarkah, D., Blades, M., Collins, A., 2024. Origin and significance of age variability in the glauconite reference material GL-O: implications for in situ Rb–Sr geochronology. Geostand. Geoanal. Res. https://doi.org/10.1111/ggr.12588.
Longerich, H. (2008). Laser ablation-inductively coupled plasma-mass spectrometry: An introduction. Laser-Ablation-ICP-MS in the Earth Sciences: *Current Practices and Outstanding Issues*, 40, 1-18. Springer.
López-Quirós, A., Sánchez-Navas, A., Nieto, F., Escutia, C., 2020. New insights into the nature of glauconite. Am. Mineral. 105 (5), 674–686. https://doi.org/10.2138/am-2020-7341.
Maidment, D.W., Williams, I.S., Hand, M., 2007. Testing long-term patterns of basin sedimentation by detrital zircon geochronology, centralian superbasin, Australia. Basin Res. 19 (3), 335–360. https://doi.org/10.1111/j.1365-2117.2007.00326.x.
Mapstone, N.B., Mcllroy, D., 2006. Ediacaran fossil preservation: taphonomy and diagenesis of a discoid biota from the Amadeus Basin, central Australia. Precambr. Res. 149 (3–4), 126–148. https://doi.org/10.1016/j.precamres.2006.05.007.
Mcdonough, W.F., Sun, S.S., 1995. The composition of the Earth. Chem. Geol. 120 (3–4), 223–253. https://doi.org/10.1016/0009-2541(94)00140-4.
Meunier, A., El Albani, A., 2007. The glauconite-Fe-illite-Fe-smectite problem: a critical review. Terra Nova 19 (2), 95–104. https://doi.org/10.1111/j.1365-3121.2006.00719.x.
Mokgalaka, N., Gardea-Torresdey, J., 2006. Laser ablation inductively coupled plasma mass spectrometry: principles and applications. Appl. Spectrosc. Rev. 41 (2), 131–150. https://doi.org/10.1080/05704920500510703.
Monchal, V., Drost, K., Chew, D., 2023. Precise U–Pb dating of incremental calcite slickenfiber growth: evidence for far-field eocene fold reactivation in Ireland. Geology 51 (7), 611–615. https://doi.org/10.1130/G50906.1.
Morton, J. G. G., Drexel, J. F. (1997). *The petroleum geology of South Australia. Vol 3: Officer Basin*. South Australia: Department of Mines and Energy Resources. Report Book, 97/19.
Neofitu, R., Mark, C., O'Connell, S., Zack, T., Rösel, D., Mark, D., Barfod, D., Flowerdew, M.J., Kelley, S., Daly, J.S., 2024. Dynamic collapse and regrowth of the Antarctic ice sheet in the Weddell Sea sector during the middle miocene: a novel

multi-proxy sedimentary provenance approach using in-situ $^{87}Rb/^{87}Sr$ dating of detrital K-feldspar. Earth Planet. Sci. Lett. 641. https://doi.org/10.1016/j.epsl.2024.118824.

Nutman, A.P., Bennett, V.C., Friend, C.R.L., Van Kranendonk, M.J., Chivas, A.R., 2016. Rapid emergence of life shown by discovery of 3,700-million-year-old microbial structures. Nature 537 (7621), 535–538. https://doi.org/10.1038/nature19355.

Odin, G.S., Dodson, M.H., 1982. Zero isotopic age of glauconies. In: Odin, G.S. (Ed.), Numerical Dating in Stratigraphy (chapter, 14. Wiley Interscience, pp. 277–305.

Odin, G., Matter, A., 1981. Origin of glauconites. Sedimentology 28 (5), 611–641.

Pourmand, A., Dauphas, N., Ireland, T.J., 2012. A novel extraction chromatography and MC-ICP-MS technique for rapid analysis of REE, sc and Y: revising CI-chondrite and post-archean australian shale (PAAS) abundances. Chem. Geol. 291, 38–54. https://doi.org/10.1016/j.chemgeo.2011.08.011.

Rafiei, M., Löhr, S.C., Alard, O., Baldermann, A., Farkaš, J., Brock, G.A., 2023. Microscale petrographic, trace element, and isotopic constraints on glauconite diagenesis in altered sedimentary sequences: implications for glauconite geochronology. Geochem. Geophys. Geosyst. 24 (4), e2022GC010795. https://doi.org/10.1029/2022GC010795.

Ravizza, G., Turekian, K.K., 1989. Application of the ^{187}Re-^{187}Os system to black shale geochronometry. Geochimica et Cosmochimica Acta 53 (12), 3257–3262. https://doi.org/10.1016/0016-7037(89)90105-1.

Redaa, A., Farkaš, J., Gilbert, S., Collins, A.S., Löhr, S., Vasegh, D., Forster, M., Blades, M., Zack, T., Giuliani, A., 2022. Testing Nano-Powder and fused-glass mineral reference materials for in situ Rb-Sr dating of glauconite, phlogopite, biotite and Feldspar via LA-ICP-MS/MS. Geostand. Geoanal. Res. 47 (1), 23–48. https://doi.org/10.1111/ggr.12467.

Redaa, A., Farkaš, J., Gilbert, S., Collins, A.S., Wade, B., Löhr, S., Zack, T., Garbe-Schönberg, D., 2021. Assessment of elemental fractionation and matrix effects during in situ Rb–Sr dating of phlogopite by LA-ICP-MS/MS: implications for the accuracy and precision of mineral ages. J. Anal. At. Spectrom 36 (2), 322–344. https://doi.org/10.1039/d0ja00299b.

Rieder, M., Cavazzini, G., D'Yakonov, Y.S., Frank-Kamenetskii, V.A., Gottardi, G., Guggenheim, S., Koval', P.W., Müller, G., Neiva, A.M.R., Radoslovich, E.W., Robert, J.-L., Sassi, F.P., Takeda, H., Weiss, Z., Wones, D.R., 1998. Nomenclature of the micas. Clay Clay Miner. 46 (5), 586–595. https://doi.org/10.1346/ccmn.1998.0460513.

Roberts, N.M.W., Drost, K., Horstwood, M.S.A., Condon, D.J., Chew, D., Drake, H., Milodowski, A.E., McLean, N.M., Smye, A.J., Walker, R.J., 2020. Laser ablation inductively coupled plasma mass spectrometry (LA–ICP–MS) U–Pb carbonate geochronology: strategies, progress, and limitations. Geochronology 2 (1), 33–61. https://doi.org/10.5194/gchron-2-33-2020.

Rollet, N., Hannaford, C., Norton, C., Kelman, A., Bishop, C., 2024. Compiling biostratigraphic and borehole stratigraphic correlation data in the Amadeus, Georgina, officer, South Nicholson and southern McArthur basins- compilation of existing data and knowledge in a common stratigraphic framework (record 2024/49). Geoscience Australia, Canberra. https://doi.org/10.26186/149317.

Rooney, A.D., Cantine, M.D., Bergmann, K.D., Gómez-Pérez, I., Al Baloushi, B., Boag, T. H., Busch, J.F., Sperling, E.A., Strauss, J.V., 2020. Calibrating the coevolution of Ediacaran life and environment. Proc. Natl. Acad. Sci. 117 (29), 16824–16830.

Schilling, J.G., Winchester, J., 1967. Rare-earth fractionation and magmatic processes. Mantles of the Earth and Terrestrial Planets 67, 267.

Scrimgeour IR, 2013. Chapter 12: Aileron Province: in Ahmad M. and Munson T.J. (compilers). *Geology and Mineral Resources of the Northern Territory* (Special Publication 5). Northern Territory Geological Survey. https://geoscience.nt.gov.au/gemis/ntgsjspui/handle/1/81492.

Smrzka, D., Zwicker, J., Bach, W., Feng, D., Himmler, T., Chen, D., Peckmann, J., 2019. The behavior of trace elements in seawater, sedimentary pore water, and their incorporation into carbonate minerals: a review. Facies 65 (4), 1–47. https://doi.org/10.1007/s10347-019-0581-4.

Środoń, J., Williams, L., Szczerba, M., Zaitseva, T., Bojanowski, M.J., Marciniak-Maliszewska, B., Kuligiewicz, A., Starzec, K., Ciesielska, Z., Paszkowski, M., 2023. Mechanism of late diagenetic alteration of glauconite and implications for geochronology. Geochim. Cosmochim. Acta 352, 157–174. https://doi.org/10.1016/j.gca.2023.05.010.

Strickler, M.E., Ferrell, R.E., 1990. Fe substitution for al in glauconite with increasing diagenesis in the first wilcox sandstone (lower eocene), Livingston Parish, Louisiana. Clay Clay Miner. 38 (1), 69–76. https://doi.org/10.1346/CCMN.1990.0380110.

Subarkah, D., Blades, M.L., Collins, A.S., Farkas, J., Gilbert, S., Löhr, S.C., Redaa, A., Cassidy, E., Zack, T., 2022. Unraveling the histories of proterozoic shales through Rb–Sr dating and trace element laser ablation analysis. Geology 50 (1), 66–70. https://doi.org/10.1130/G49187.1.

Subarkah, D., Nixon, A.L., Gilbert, S.E., Collins, A.S., Blades, M.L., Simpson, A., Lloyd, J. C., Virgo, G.M., Farkas, J., 2024. Double dating sedimentary sequences using new applications of in-situ laser ablation analysis. Lithos 480–481, 107649. https://doi.org/10.1016/j.lithos.2024.107649.

Tingate, P.R., Duddy, I.R., 2002. The thermal history of the eastern Officer Basin (South Australia): evidence from apatite fission track analysis and organic maturity data. Tectonophysics 349 (1–4), 251–275. https://doi.org/10.1016/S0040-1951(02)00056-2.

Vermeesch, P., 2018. IsoplotR: a free and open toolbox for geochronology. Geosci. Front. 9 (5), 1479–1493. https://doi.org/10.1016/j.gsf.2018.04.001.

Villa, I.M., De Bièvre, P., Holden, N.E., Renne, P.R., 2015. IUPAC-IUGS recommendation on the half-life of 87Rb. Geochimica et Cosmochimica Acta 164, 382–385. https://doi.org/10.1016/j.gca.2015.05.025.

Walter, M.R., Veevers, J.J., Calver, C.R., Grey, K., 1995. Neoproterozoic stratigraphy of the centralian superbasin, Australia. Precambr. Res. 73 (1–4), 173–195. https://doi.org/10.1016/0301-9268(94)00077-5.

Webster, L.J., Hill, A.C., Grey, K., Gostin, V.A., 2004. New records of late neoproterozoic acraman ejecta in the Officer Basin. Aust. J. Earth Sci. 51 (1), 47–51. https://doi.org/10.1046/j.1400-0952.2003.01044.x.

Williams, C.T., Henderson, P., Marlow, C.A., Molleson, T.I., 1997. The environment of deposition indicated by the distribution of rare earth elements in fossil bones from Olduvai Gorge, Tanzania. Appl. Geochem. 12 (4), 537–547.

Williams, G.E., Gostin, V.A., 2005. Acraman–Bunyeroo impact event (Ediacaran), South Australia, and environmental consequences: twenty-five years on. Aust. J. Earth Sci. 52 (4–5), 607–620. https://doi.org/10.1080/08120090500181036.

Williams, G.E., Schmidt, P.W., 2018. Shuram–Wonoka carbon isotope excursion: ediacaran revolution in the world ocean's meridional overturning circulation. Geoscience Frontiers 9 (2), 391–402. https://doi.org/10.1016/j.gsf.2017.11.006.

Willman, S., Moczydłowska, M., 2008. Ediacaran acritarch biota from the Giles 1 drillhole, Officer Basin, Australia, and its potential for biostratigraphic correlation. Precambr. Res. 162 (3–4), 498–530. https://doi.org/10.1016/j.precamres.2007.10.010.

Wilson, C.J.L., 2021. Tectonic history related to the southern section of the kalinjala Shear zone, Eyre peninsula, South Australia: and correlations with terre adelie craton, Antarctica. Gondw. Res. 98, 17–45. https://doi.org/10.1016/j.gr.2021.05.018.

Yang, B., Smith, T.M., Collins, A.S., Munson, T.J., Schoemaker, B., Nicholls, D., Cox, G., Farkas, J., Glorie, S., 2018. Spatial and temporal variation in detrital zircon age provenance of the hydrocarbon-bearing upper roper group, beetaloo sub-basin, Northern Territory, Australia. Precambr. Res. 304, 140–155. https://doi.org/10.1016/j.precamres.2017.10.025.

Yin, L., Zhao, P., Liu, J., Li, J., 2023. Re-Os isotope system in organic-rich samples for dating and tracing: methodology, principle, and application. Earth Sci. Rev. 238, 104317. https://doi.org/10.1016/j.earscirev.2023.104317.

Zack, T., Hogmalm, J., 2016. Laser ablation Rb/Sr dating by online chemical separation of Rb and Sr in an oxygen-filled reaction cell. Chem. Geol. 437, 120–133. https://doi.org/10.1016/j.chemgeo.2016.05.027.

Zang, W.L., 1995. Early neoproterozoic sequence stratigraphy and acritarch biostratigraphy, eastern Officer Basin, South Australia. Precambr. Res. 74 (3), 119–175. https://doi.org/10.1016/0301-9268(95)00007-R.

Zhang, L., Algeo, T.J., Cao, L., Zhao, L., Chen, Z.-Q., Li, Z., 2016. Diagenetic uptake of rare earth elements by conodont apatite. Palaeogeogr. Palaeoclimatol. Palaeoecol. 458, 176–197. https://doi.org/10.1016/j.palaeo.2015.10.049.